

DETECTION OF HIGHLY IONIZED METAL ABSORPTION LINES IN THE ULTRACOMPACT X-RAY DIPPER 4U 1916–05

ADRIENNE M. JUETT¹ AND DEEPTO CHAKRABARTY²

Accepted for publication in the Astrophysical Journal

ABSTRACT

We present the high-resolution *Chandra X-ray Observatory* persistent (non-dip) spectrum of 4U 1916–05 which revealed narrow absorption lines from hydrogenic neon, magnesium, silicon, and sulfur, in addition to the previous identified hydrogenic and helium-like iron absorption lines. This makes 4U 1916–05 only the second of the classical X-ray dipper systems to show narrow absorption lines from elements other than iron. We propose two possible explanations for the small measured line widths ($\lesssim 500\text{--}2000\text{ km s}^{-1}$), compared to the expected Keplerian velocities ($> 1000\text{ km s}^{-1}$) of the accretion disk in this 50-min orbital period system, and lack of wavelength shifts ($\lesssim 250\text{ km s}^{-1}$). First, the ionized absorber may be stationary. Alternatively, the line properties may measure the relative size of the emission region. From this hypothesis, we find that the emission region is constrained to be $\lesssim 0.25$ times the radial extent of the absorber. Our results also imply that the ionized absorber spans a range of ionization parameters.

Subject headings: binaries: close — stars: individual (4U 1916–05) — X-rays: binaries

1. INTRODUCTION

It was anticipated that high-resolution spectra of low-mass X-ray binaries (LMXBs) would reveal a wealth of line features which could be used to better understand accretion disk structure, but such features have been largely absent in most *Chandra X-ray Observatory* and *XMM-Newton* spectra of LMXBs. One exception is the class of X-ray dippers. X-ray dippers show intensity dips, although not necessarily eclipses, on the orbital period and have inclination angles in the range $60^\circ < i < 80^\circ$. The dipping behavior is caused by absorption of the continuum by the accretion disk or its atmosphere.

The best studied of the X-ray dippers, the neutron star (NS) binary, EXO 0748–676 ($P_{\text{orb}}=3.8\text{ hr}$), showed emission lines from the hydrogenic and helium-like species of nitrogen, oxygen, neon, magnesium, and silicon in its *XMM* and *Chandra* spectra (Cottam et al. 2001; Jimenez-Garate et al. 2003). The *XMM* spectrum of the X-ray dipper MXB 1659–298 ($P_{\text{orb}}=7.1\text{ hr}$) showed narrow absorption lines from highly ionized oxygen, neon, and iron, and a broad Fe-*K* emission line (Sidoli et al. 2001). *XMM* data from four other dippers, X1624–490 ($P_{\text{orb}}=21.0\text{ hr}$), 4U 1254–69 ($P_{\text{orb}}=3.9\text{ hr}$), 4U 1916–05 ($P_{\text{orb}}=0.83\text{ hr}$), and 4U 1323–62 ($P_{\text{orb}}=2.94\text{ hr}$) revealed similar narrow iron absorption lines and some evidence for broad iron emission lines (Parmar et al. 2002; Boirin & Parmar 2003; Boirin et al. 2004, 2005; Church et al. 2005).

The presence of these absorption features in X-ray dippers, but not in other LMXBs, has led to the suggestion that the absorbing material has a cylindrical distribution (e.g., Boirin et al. 2004). The lack of variation in the properties of the absorption lines as a function of orbital phase, excluding the dipping region, implies an

azimuthal symmetry (see, e.g., Boirin et al. 2004, and references therein). This in turn points to some relationship between the accretion disk and the absorbing material.

In this paper, we present the high-resolution *Chandra* spectrum of 4U 1916–05, the shortest orbital period X-ray dipper. The 50-min orbital period of 4U 1916–05 was discovered independently by White & Swank (1982) and Walter et al. (1982) from dips seen in the X-ray emission. The stability of the dip period over many years led the authors to associate it with the orbital period of the system (but also see, Chou et al. 2001; Homer et al. 2001; Retter et al. 2002). The dipping behavior of 4U 1916–05 is variable on the order of ~ 4 days, varying from short ($\approx 10\%$ of orbital phase), shallow dips to long ($\approx 40\%$ of orbital phase), deep dips (e.g., Chou et al. 2001). Unique among the X-ray dippers, the 50-min orbital period of 4U 1916–05 places it in the class of ultracompact LMXBs which require hydrogen-deficient and/or degenerate donors (e.g., Joss et al. 1978). It has been proposed that the companion is a hydrogen-deficient but not yet degenerate star (Nelson et al. 1986). Observational evidence points to a helium-rich donor. The X-ray burst properties of 4U 1916–05 suggest that the accreting material is helium-rich and that the distance to 4U 1916–05 is $8.9 \pm 1.3\text{ kpc}$ (Galloway et al. 2005, in prep.). A recent optical spectrum of 4U 1916–05 shows a feature at 4540 \AA which may be due to He II (Nelemans & Jonker 2005).

The non-dip spectrum can be fit with a power-law or power-law + blackbody model in the range 0.5–10 keV. Variations in the best-fit spectral parameters are correlated with the broad-band luminosity and the position of 4U 1916–05 in its color-color diagram (Bloser et al. 2000). In addition, Asai et al. (2000) detected a broad (FWHM = 0.7 keV) emission feature in the *ASCA* spectrum at 5.9 keV with an equivalent width of 87 eV attributed to Fe-*K* emission. Highly ionized iron absorption lines were found in the *XMM* spectrum of

¹ Department of Astronomy, University of Virginia, Charlottesville, VA 22903; ajuett@virginia.edu

² Department of Physics and Kavli Institute for Astrophysics and Space Research, Massachusetts Institute of Technology, Cambridge, MA 02139; deeppto@space.mit.edu

4U 1916–05 with marginal detections of other highly ionized features (e.g., Mg XII, S XVI; Boirin et al. 2004).

2. OBSERVATIONS AND DATA REDUCTION

We observed 4U 1916–05 on 2004 August 07 for 50 ks with *Chandra* using the High Energy Transmission Grating Spectrometer (HETGS) and the Advanced CCD Imaging Spectrometer (ACIS; Canizares et al. 2005). The HETGS carries two transmission gratings: the Medium Energy Gratings (MEGs) with a range of 2.5–31 Å (0.4–5.0 keV) and the High Energy Gratings (HEGs) with a range of 1.2–15 Å (0.8–10.0 keV). The HETGS spectra are imaged by ACIS, an array of six CCD detectors. The HETGS/ACIS combination provides both an undispersed (zeroth order) image and dispersed spectra from the gratings. The various orders overlap and are sorted using the intrinsic energy resolution of the ACIS CCDs. The first-order MEG (HEG) spectrum has a spectral resolution of $\Delta\lambda = 0.023$ Å (0.012 Å). To reduce pileup, the observation used a sub-array of 512 rows, yielding a frametime of 1.7 s. The “level 1” event files were processed using the CIAO v3.2 data analysis package³. The standard CIAO spectral reduction procedure was performed.

The combined MEG + HEG first order dispersed spectrum of 4U 1916–05 has an average count rate of 10.6 ± 1.3 cts s^{-1} . During our observation, 4U 1916–05 showed only mild dipping behavior as well as two X-ray bursts (see Figure 1). In the analysis presented here, we focus only on the persistent (non-dip) emission from 4U 1916–05. We inspected the lightcurve at times of expected dipping, using the dip ephemeris of Chou et al. (2001). Of the 16 orbital cycles covered by our observation, only six showed statistically significant dipping behavior. These dips were centered on a phase of ≈ 0.15 and had width of ≈ 0.15 in phase. To produce our persistent (non-dip) spectrum, we excluded data from phases 0.0–0.3 for all orbital cycles. In addition, we excluded data during the two X-ray bursts. We filtered the level 2 event file, yielding a persistent (non-dip, non-burst) exposure time of 31 ks. We then extracted source and background spectra for both the plus and minus first order MEG and HEG. Detector response files (RMFs and ARFs) were created for the four spectra using the standard CIAO tools.

For bright sources, pileup can be a problem for CCD detectors (see, e.g., Davis 2003). We checked the dispersed spectra of 4U 1916–05 and found signs of pileup in the first order MEG spectrum. In dispersed spectra, pileup can affect only a limited wavelength range, particularly where the effective area of the instrument is the highest. In our observation, pileup was present between 2–10 Å in the MEG plus and minus first orders. No pileup was found in the HEG spectra.

The spectral analysis was performed using ISIS (Houck & Denicola 2000). The +1 and –1 order spectra were combined for the HEG and MEG respectively using the ISIS function `combine_datasets`. This function is similar to summing the datasets, but more accurately takes into account the different responses for each dataset. We fit jointly the HEG spectra over the range 1.6–11.5 Å and MEG spectra over the range 10.0–14.0 Å.

³ <http://asc.harvard.edu/ciao/>

3. ANALYSIS AND RESULTS

An initial inspection of the spectrum of 4U 1916–05 revealed narrow absorption features at 12.1, 8.4, 6.2, and 4.7 Å (see Figure 2), attributable to hydrogenic neon, magnesium, silicon, and sulfur. To determine the continuum model, we fit the spectrum ignoring regions around these lines as well as the Fe-*K* region at 1.8 Å. We tested three different continuum models: power law, power law + blackbody, and power law + disk blackbody, all with interstellar absorption as described by the `tbabs` model using the abundances of Wilms et al. (2000). Both the power law + blackbody and power law + disk blackbody models give better fits to the data than the power law alone (see Table 1). We take the power law + disk blackbody model as the continuum model, although we note that the choice of the power law + blackbody model would make little difference to our results. The absorbed 0.5–10 keV flux from 4U 1916–05 was 8.0×10^{-10} erg cm^{-2} s^{-1} .

Our best-fit model is significantly different from that found by Boirin et al. (2004). But as noted by Boirin et al. (2004), the limited energy range covered by *XMM* and *Chandra* make it difficult to determine a unique solution to the continuum fit. One interesting difference between our *Chandra* data and the *XMM* data, is the presence of an edge at 0.98 keV. Boirin et al. (2004) found that both the EPIC and RGS data were best-fit when an edge, with depth $\tau = 0.11 \pm 0.03$, was included. In contrast, the addition of an edge at 0.98 keV does not improve the chi-squared value of the continuum fit for the *Chandra* data. We find an upper limit of $\tau < 0.08$ for the edge, barely consistent with the *XMM* result. The 0.5–10 keV luminosity of 4U 1916–05 was 9.0×10^{36} erg s^{-1} , using a distance of 8.9 kpc, during the *Chandra* observation. This is ≈ 2 times greater than found during the *XMM* observation (Boirin et al. 2004).

With the best-fit continuum model fixed, we fit the lines from Ne X, Mg XII, Si XIV, S XVI, Fe XXV, and Fe XXVI with Gaussian models to determine the line positions, widths, and fluxes. In addition, we determined the upper limits to the flux from the helium-like ions of neon, magnesium, silicon, and sulfur. For the upper limit measurements, we fixed the wavelength to those given in Behar & Netzer (2002) and we fixed the line width $\sigma = 0.005$ Å. We marginally detected the helium-like ion of sulfur. The neon lines were covered by the MEG spectrum, while the rest of the lines were located in the HEG spectral region. The best-fit parameters are given in Table 2 and the spectra and best-fit models are shown in Figures 3 and 4.

The line positions are consistent with the rest frame wavelengths of hydrogenic neon, magnesium, silicon, and sulfur, and hydrogenic and helium-like iron. This suggests that there is no bulk motion along our line of sight associated with the absorbing material. In addition, the measured line widths are comparable to, or less than, the instrument resolution (0.023 Å for MEG, 0.012 Å for HEG). Therefore, direct measurements of the velocity widths, or temperature, of the absorbing material are not possible with these data. The derived temperature limits range from $< 4 \times 10^8$ K for Mg XII, to $1.2 \pm 1.1 \times 10^{10}$ K for Fe XXVI.

From the best fit equivalent widths (EW), we can esti-

mate the column density (N_Z) of the ions using the relationship between EW, N_Z , and the transition oscillator strength f_{ij}

$$\frac{W_\lambda}{\lambda} = \frac{\pi e^2}{m_e c^2} N_Z \lambda f_{ij} = 8.85 \times 10^{-13} N_Z \lambda f_{ij}, \quad (1)$$

where W_λ is the EW in wavelength units and λ , the line wavelength, is given in cm units (Spitzer 1978). The equation above is true only when a line is unsaturated, on the linear part of the curve of growth. For saturated lines, the exact relationship between EW and N_Z becomes a more complicated function, and includes a dependence on the velocity of the ions. We used the oscillator strengths given by Verner et al. (1996) for the hydrogenic lines, and those of Behar & Netzer (2002) for the helium-like lines. Our results are given in Table 2. If the lines are saturated, the values represent a lower limit to the column densities for each ion.

Comparing our results with those of Boirin et al. (2004), we find that the iron line EWs are barely consistent within the errors. Our Fe XXVI EW is at the upper limit of the *XMM* result, while our Fe XXV EW is at the lower limit. It is possible that the greater luminosity of 4U 1916–05 during the *Chandra* observation has caused a real difference in the Fe XXV and Fe XXVI column densities, compared to the lower luminosity *XMM* data, but the difference is not significant enough to confirm this. The iron line widths found in the *Chandra* data are lower than the upper limits found in the *XMM* data owing to the higher resolution of the HETG compared to the EPIC pn. Our EW measurements for S XVI and Ne X are consistent with the values reported for the *XMM* data, but our Mg XII EW is significantly below the result of Boirin et al. (2004). We note however that Boirin et al. (2004) concluded that their Mg XII detection was only marginal, therefore the difference between the *Chandra* and *XMM* results may not indicate a real change between the two observations. As in the other X-ray dipper observations, we found no variation in the line parameters as a function of orbital phase (see Figure 5).

4. DISCUSSION

Our *Chandra*/HETGS observation of 4U 1916–05 revealed narrow, unresolved absorption lines in the persistent emission, attributable to hydrogenic neon, magnesium, silicon, and sulfur, in addition to the previous identified hydrogenic and helium-like iron absorption lines. This makes 4U 1916–05 only the second of the classical X-ray dipper systems to show narrow absorption lines from mid- Z elements (Boirin et al. 2004, and references therein).

The properties of these lines is of particular interest for understanding the emission and absorption processes. With a 50 min orbital period, 4U 1916–05 is the shortest period X-ray dipper, and as such should have the smallest accretion disk. If the lines are associated with the accretion disk, they should have widths comparable to the expected Keplerian velocities in the disk. Assuming a 1.4–2.0 M_\odot primary and a 0.1–0.15 M_\odot secondary (see, e.g. Nelson et al. 1986), we can estimate the outer disk velocity assuming that the disk fills 70% of the primary Roche lobe. We find that the outer disk velocity should be in the range of 1000–1300 km s⁻¹, while the companion velocity should be 740–840 km s⁻¹. In all cases, the

measured line widths are consistent with, or below, the instrument resolution. For Mg XII and Fe XXV, the upper limits on the line widths are less than the estimated outer disk velocity. Additionally, we measure no shift in the wavelength of the lines, ruling out a strong outflow. The S XVI line shows a slight shift (+0.004 Å) but given that this is the least significant of our line detections and the possibility of systematic errors, we do not feel it is a significant result.

We suggest two possible explanations for these results. First, the absorber could be static, producing the narrow lines and lack of wavelengths shifts. This however seems unlikely given the large quantities of angular momentum present in the system. Instead, we propose that the line properties are a measure of the emission properties, particularly the extent of the emission. In this case, we assume that the ionized absorber is associated with either the accretion disk or its atmosphere, as suggested by the implied cylindrical geometry (see e.g., Boirin et al. 2004). The rotation of the absorbing material is only measurable when it has a component along the line of sight to the emitter. If the bulk velocity is perpendicular to the line of sight, no velocity effects will be found in the absorption lines (excluding thermal or turbulent motions which we take as small compared to the Keplerian velocities in the disk). From the limits on the linewidths, we can calculate the maximum allowable radial extent of the emitter. We find that the X-ray emission region is $\lesssim 32000$ km, assuming that the absorber is located at the outer edge of the accretion disk. This represents the maximum upper limit on the extent. We note that if the absorber is located at a smaller disk radius, the upper limit will be smaller, roughly 1/4 of the absorber radius.

Assuming that photoionization is the dominant ionization process for the absorbing material, we can estimate the ionization parameter, $\xi = L/n_e r^2$ (Tarter et al. 1969), from the ratio of the helium-like to hydrogenic column densities for each atomic species. We assume that the helium-like and hydrogenic ions are present at the same, single-valued ionization parameter. This is a simple approximation to the expected true state of the system in which the ions exist in different relative proportions over a range of ionization parameters.

We used XSTAR⁴ to estimate the ion abundances as a function of ξ for an optically thin plasma, with constant number density and solar abundances. We note that while the companion in 4U 1916–05 is expected to be a hydrogen-deficient star, and solar abundances would therefore not apply, we found that varying the abundances made no significant difference in the helium-like to hydrogenic column density ratios for any element. The only XSTAR input that made a substantial difference in the inferred ionization parameters was the shape of the input spectrum. We tried three models, a power law with $\alpha = -1$, a 10 keV bremsstrahlung, and a user defined model based on the continuum emission of 4U 1916–05.

We compared the XSTAR results with the column density ratios for neon, magnesium, silicon, sulfur, and iron as given in Table 2. We note that these values are only valid if the lines are unsaturated. The limits for neon and magnesium are too high to provide any constraint on the ionization parameter. For silicon, we find $\log \xi \gtrsim 1.7$ –2.0

⁴ <http://heasarc.gsfc.nasa.gov/docs/software/xstar/xstar.html>

and for sulfur, $\log \xi = 1.5\text{--}3.3$, given the error in the measurement and the variation in ξ with spectral model (highest values for the power law model, lower for the bremsstrahlung and user defined models). The most constraining result comes of course from the iron ratio, where we find $\log \xi = 3.50 \pm 0.13$ for the bremsstrahlung model, 3.73 ± 0.13 for the power law model, and 3.02 ± 0.12 for the user defined model. This rough estimate would suggest that the iron absorption is found in a material with higher ionization than the lower Z elements. Our result is consistent with modeling of the ionized absorber in MXB 1658–298 which required a distribution of ion-

ization parameters (Díaz Trigo et al. 2006). This is of course expected since in a material ionized enough to contain helium-like and hydrogenic iron, the lower Z elements would be completely stripped.

We thank Jonathan Gelbord, Kazunori Ishibashi, and Michael Nowak for useful discussions. We would also like to thank Tim Kallman for his help with XSTAR. We also thank the anonymous referee whose comments improved the paper. Partial support for this work was provided by NASA through Chandra award number GO4-5054X.

REFERENCES

- Asai, K., Dotani, T., Nagase, F., & Mitsuda, K. 2000, *ApJS*, 131, 571
- Behar, E., & Netzer, H. 2002, *ApJ*, 570, 165
- Bloser, P. F., Grindlay, J. E., Barret, D., & Boirin, L. 2000, *ApJ*, 542, 989
- Boirin, L., Méndez, M., Díaz Trigo, M., Parmar, A. N., & Kaastra, J. S. 2005, *A&A*, 436, 195
- Boirin, L., & Parmar, A. N. 2003, *A&A*, 407, 1079
- Boirin, L., Parmar, A. N., Barret, D., Paltani, S., & Grindlay, J. E. 2004, *A&A*, 418, 1061
- Canizares, C. R., et al. 2005, *PASP*, 117, 1144
- Chou, Y., Grindlay, J. E., & Bloser, P. F. 2001, *ApJ*, 549, 1135
- Church, M. J., Reed, D., Dotani, T., Bałucińska-Church, M., & Smale, A. P. 2005, *MNRAS*, 359, 1336
- Cottam, J., Kahn, S. M., Brinkman, A. C., den Herder, J. W., & Erd, C. 2001, *A&A*, 365, L277
- Davis, J. E. 2003, in *Proceedings of the SPIE, Vol. 4851, X-Ray and Gamma-Ray Telescopes and Instruments for Astronomy*, ed. J. E. Truemper & H. D. Tananbaum, 101–111
- Díaz Trigo, M., Parmar, A. N., Boirin, L., Méndez, M., & Kaastra, J. S. 2006, *A&A*, 445, 179
- Homer, L., Charles, P. A., Hakala, P., Muhli, P., Shih, I.-C., Smale, A. P., & Ramsay, G. 2001, *MNRAS*, 322, 827
- Houck, J. C., & Denicola, L. A. 2000, in *ASP Conf. Ser. 216: Astronomical Data Analysis Software and Systems IX, Vol. 9*, 591–594
- Jimenez-Garate, M. A., Schulz, N. S., & Marshall, H. L. 2003, *ApJ*, 590, 432
- Joss, P. C., Avni, Y., & Rappaport, S. 1978, *ApJ*, 221, 645
- Nelemans, G., & Jonker, P. G. 2005, in *AIP Conf. Proc. 797: Interacting Binaries: Accretion, Evolution and Outcomes*, ed. L. A. Antonelli et al., 396–401
- Nelson, L. A., Rappaport, S. A., & Joss, P. C. 1986, *ApJ*, 304, 231
- Parmar, A. N., Oosterbroek, T., Boirin, L., & Lumb, D. 2002, *A&A*, 386, 910
- Retter, A., Chou, Y., Bedding, T. R., & Naylor, T. 2002, *MNRAS*, 330, L37
- Sidoli, L., Oosterbroek, T., Parmar, A. N., Lumb, D., & Erd, C. 2001, *A&A*, 379, 540
- Spitzer, L. 1978, *Physical processes in the interstellar medium* (New York: Wiley-Interscience)
- Tarter, C. B., Tucker, W. H., & Salpeter, E. E. 1969, *ApJ*, 156, 943
- Verner, D. A., Verner, E. M., & Ferland, G. J. 1996, *Atomic Data and Nuclear Data Tables*, 64, 1
- Walter, F. M., Bowyer, S., Mason, K. O., Clarke, J. T., Henry, J. P., Halpern, J., & Grindlay, J. E. 1982, *ApJ*, 253, L67
- White, N. E., & Swank, J. H. 1982, *ApJ*, 253, L61
- Wilms, J., Allen, A., & McCray, R. 2000, *ApJ*, 542, 914

TABLE 1. BEST-FIT CONTINUUM SPECTRAL PARAMETERS^a

Model	N_{H} (10^{21} cm ⁻²)	Γ	A_1^{b}	kT (keV)	Norm ^c	χ^2_{ν}/ν
PL	6.9±0.2	1.519±0.019	12.2±0.3	1.123/1187
PL+BB	5.6±0.7	1.31±0.11	8.5±1.7	0.54±0.04	70±30	1.114/1185
PL+DISKBB	5.4±0.7	1.0±0.4	5±3	0.91±0.11	15±5	1.113/1185

^aAll errors quoted at the 90%-confidence level.

^bPower-law normalization in units of 10^{-2} photons cm⁻² s⁻¹ keV⁻¹.

^cThermal component normalization. For the blackbody model, norm = $R_{\text{km}}^2/D_{10\text{kpc}}^2$; for the disk blackbody model, norm = $(R_{\text{in,km}}/D_{10\text{kpc}})^2 \cos \theta$, where θ is the inclination angle of the disk.

 TABLE 2. BEST-FIT LINE PARAMETERS^a

Ion	Wavelength (Å)	FWHM (Å)	FWHM (km s ⁻¹)	EW (mÅ)	N_{Z}^{b} (10^{16} cm ⁻²)
Ne X	12.140±0.006	0.035±0.019	870±470	-25±8	4.6±1.5
Mg XII	8.425±0.002	<0.014	<500	-9±3	3.4±1.1
Si XIV	6.185±0.002	0.016±0.009	800±460	-11±3	8±2
S XVI	4.736±0.003	0.012±0.009	750±600	-7±3	8±4
Fe XXV	1.8519±0.0017	<0.005	<950	-4.9±1.1	20±5
Fe XXVI	1.7811±0.0015	0.012±0.005	1900±900	-11±3	90±30
Upper Limits on Helium-like Ions					
Ne IX	13.448 (fixed)	0.012 (fixed)	260 (fixed)	> -9	< 0.9
Mg XI	9.170 (fixed)	0.012 (fixed)	380 (fixed)	> -6	< 1.2
Si XIII	6.648 (fixed)	0.012 (fixed)	530 (fixed)	> -3	< 1.1
S XIV	5.039 (fixed)	0.012 (fixed)	700 (fixed)	-4±3	2.5±1.9

^aAll errors quoted at the 90%-confidence level.

^bAssumes lines are unsaturated. Values represent a lower limit to the column density if lines are saturated.

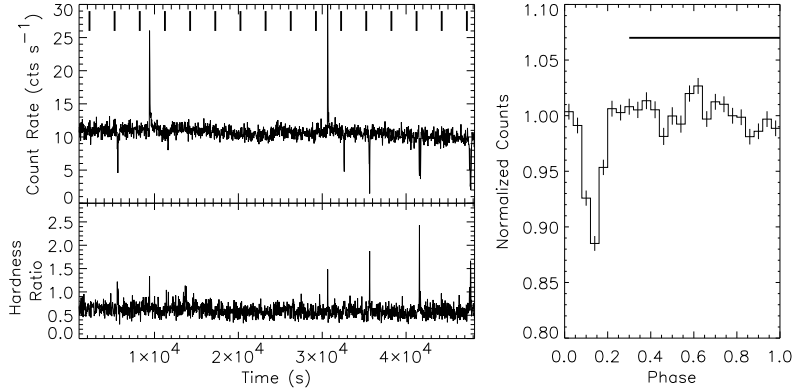


FIG. 1.— *Left panel, top*: First order HEG+MEG 0.5–8.0 keV count rate over the *Chandra* observation of 4U 1916–05. The solid marks at the top of the figure indicate the expected dip times using the dip ephemeris of Chou et al. (2001). *Left panel, bottom*: The hardness ratio ([4–8 keV count rate]/[0.5–1.5 keV count rate]) during the observation. As expected the hardness ratio increases during the X-ray dips (due to low energy absorption) and X-ray bursts. *Right Panel*: Normalized phase folded lightcurve of the first order HEG+MEG 0.5–8.0 keV counts from 4U 1916–05. The times of X-ray bursts have been removed and the lightcurve has been corrected for exposure effects. The solid line from phases 0.3–1.0 indicates the data used to produce the persistent (non-dip) spectrum.

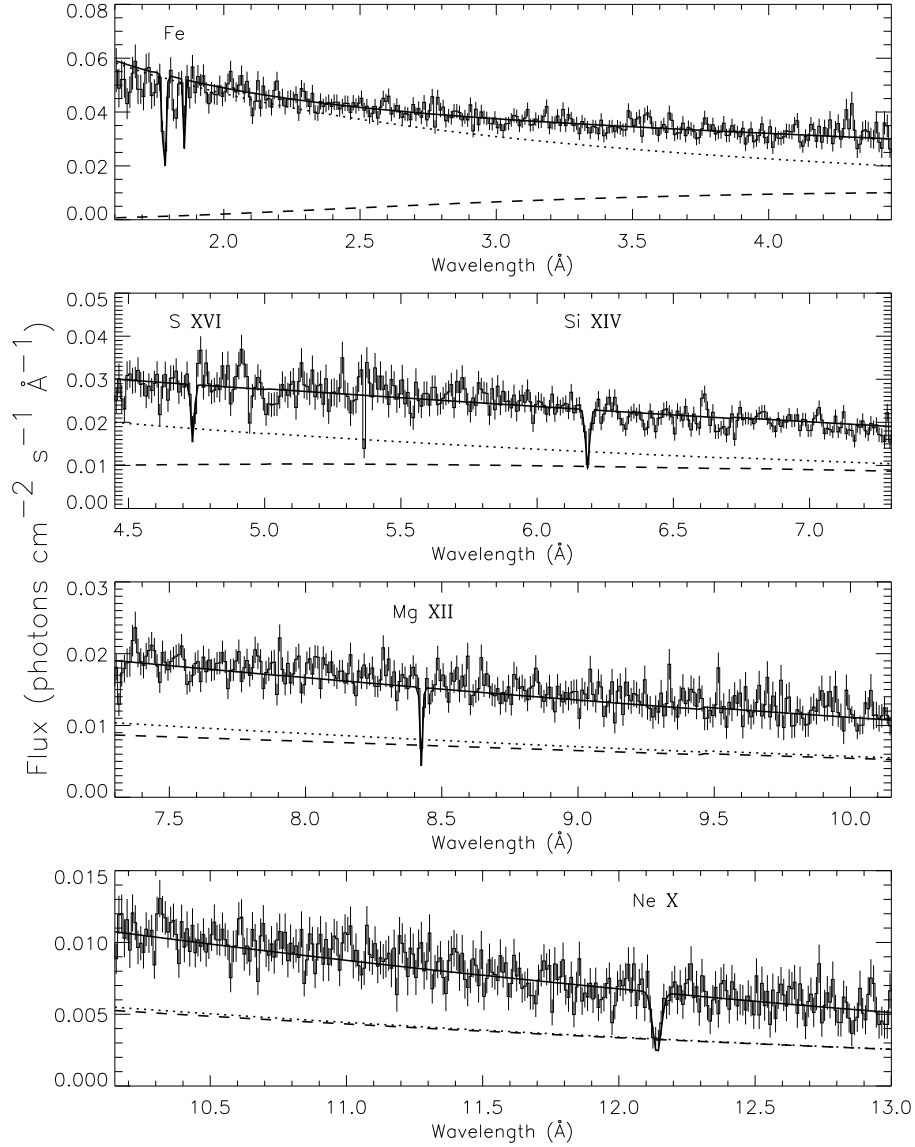


FIG. 2.— Flux spectra and best-fit model for the combined first order MEG+HEG *Chandra* spectrum of 4U 1916–05. The data and model are binned to 0.010 Å. The solid line is the full best-fit model including both continuum and line components. The dotted and dashed lines show the best-fit power law and disk blackbody continuum models, respectively. The absorption features from neon, magnesium, silicon, sulfur, and iron are labeled.

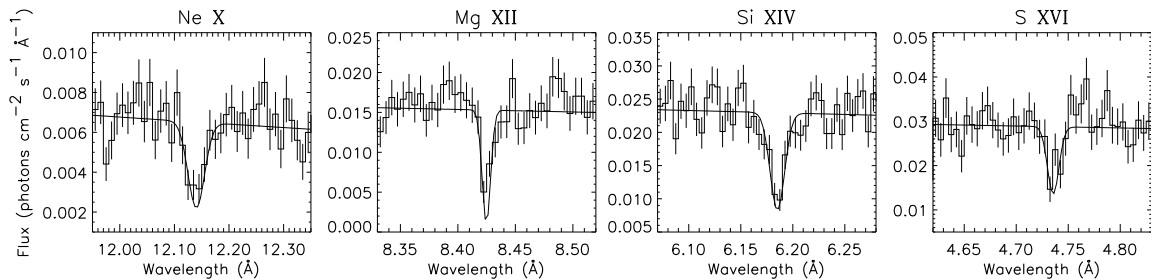


FIG. 3.— Flux spectra and best-fit models for the Ne X, Mg XII, Si XIV, and S XVI line regions. Note that the Ne X line is covered by the lower resolution MEG, while the other lines are covered by the HEG. The line-like feature at ≈ 11.97 Å in the Ne X region is more narrow than the instrument resolution and is likely an instrumental artifact.

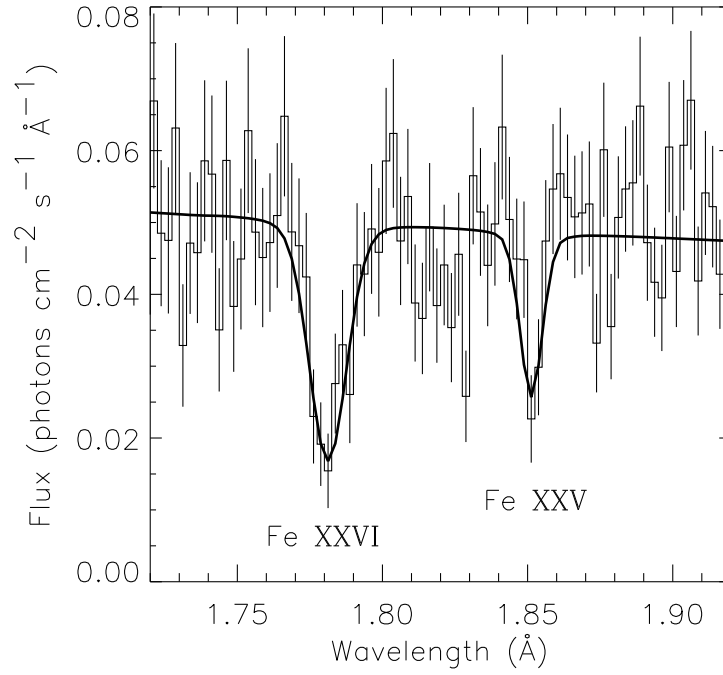


FIG. 4.— Flux spectrum and best-fit model for the iron line region. The Fe XXV line is found at 1.85 Å and the Fe XXVI line is found at 1.78 Å.

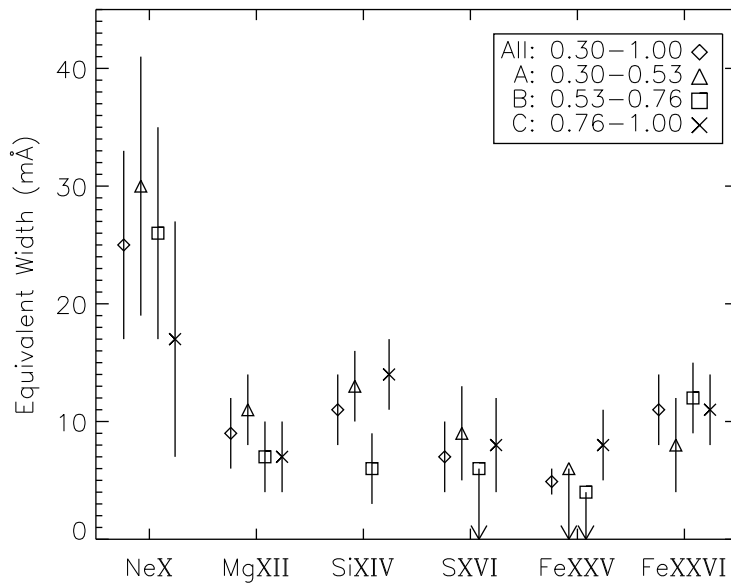


FIG. 5.— Comparison of the absorption line equivalent widths as a function of orbital phase. We plot the EWs for the full dataset (diamond), in addition to three phase groups: group A covering phases 0.30–0.53 (triangle), group B covering phases 0.53–0.76 (square), and group C covering phases 0.76–1.00 (x). No significant variation of the line properties are found.